Spatially Resolved Thermalization Dynamics of Electronically Photoexcited Azulene Probed by a Molecular Integrated Thermometer

Toshiya Okazaki, Noboru Hirota, Toshi Nagata, Atsuhiro Osuka, and Masahide Terazima*

Department of Chemistry, Graduate School of Science, Kyoto University, Kyoto 606-8502, Japan

Received: March 24, 1999; In Final Form: June 30, 1999

The vibrational cooling process of photoexcited azulene (Az) was studied by using a covalently connected molecular thermometer (coumarin 151 (C151)). The transient absorption at the red edge of the absorption band of C151 detected after the photoexcitation of azulene is attributed to the hot band absorption of C151. First, the time profile of the transient absorption signals of the integrated molecule Az−CH_2−C151 was examined by two thermalization models: one of which includes the intermolecular energy transfer through the σ-bond and through the solvent, and the other includes only the through-solvent path. From these analyses, it is found that the cooling times of azulene in the solvents used here were found to be less than 7 ps. These results indicate that there is a fast cooling process after the relaxation of the electronically excited state compared with that reported before. The transient absorption spectrum and its time profile of a compound with a longer chain (Az−$(CH_2)_3$−C151) are very similar to those of Az−CH_2−C151 except for the much weaker intensity. These facts indicate that the molecular structure of Az−$(CH_2)_3$−C151 is flexible and the distance between the thermometer (C151) and the heater (azulene) is short.

1. Introduction

The energy dissipation mechanisms by nonradiative transition from photoexcited states to the surroundings have been studied extensively.[1] Mostly, the energy dissipation has been discussed by associating it with the vibrational relaxation process. The vibrational cooling in the S_0 state of azulene is one of the extensively studied systems in a wide density region experimentally and theoretically.[2−14] After photoexcitation to the S_1 state, the vibrationally "hot" azulene in the S_0 state is produced with a lifetime of 1 ps,[15,16] and a subsequent vibrational cooling is monitored via the hot band of azulene.[6,7,9] The results showed that the vibrational cooling of azulene occurs around 10 ps. In *n*-alkanes, the cooling times decrease with increasing chain length from 12.5 ps in pentane to 10.8 ps in hexadecane. Hydrogen bond formation has a strong influence on this thermalization process. With increasing hydrogen bond density, the vibrational cooling time decreases from 9 ps in ethanol to 3.3 ps in a 3:1 mixture of water and methanol. In these studies, azulene itself acts as a molecular thermometer to monitor the molecular energy.

On the other hand, studies of the thermalization process by monitoring the temperature rise of the surrounding matrix could be another important approach.[17] This approach has been mainly used by our group using several photothermal spectroscopies.[18−23] A fast temperature rise of the surrounding solvent molecules with a few picosecond time resolution was monitored after photoexcitation of solute molecules in water[18−20] and organic solvents.[21−23]

One of important parameters, which has not been detected so far, is the spatial resolution. If we can detect the transient temperature of the solvent as a function of the distance from the solute, the thermalization process as well as the heat flow mechanism will be more clear (Figure 1a). We recently carried out the first attempt to detect the thermalization process with a high spatial resolution by using a molecular heater and a molecular thermometer integrated system (Figure 1b).[24] After photoexcitation of azulene that was used as a heater molecule, the excess energy is dissipated to the surroundings. This energy flow was monitored via a hot band absorption change of a thermometer (coumarin 151 (C151)) connected via a methylene group (Az−CH_2−C151). In the previous paper, essential features of the temperature detection by this molecular system were briefly described.[24]

In the present paper, the transient temperature with a high spatial resolution using azulene (Az) and C151 molecular integrated system is described in detail and the analysis is presented. The observed results are analyzed by two thermalization models: one includes the through-bond and the through-solvent energy transfer, and the other includes only the through-solvent energy transfer. The experimental observations can be explained either by the thermalization through both paths or only through the solvent path with a small number of directly energy accepting solvent molecules. The thermalization rates obtained from both models are rather fast (2−7 ps) and depend on the solvent. These fast thermalization rates are compared with the vibrational cooling rates measured via the hot band detection of azulene itself. The transient temperature detected by a compound in which azulene and C151 are combined with a longer chain (propylene group) (Az−$(CH_2)_3$−C151) is discussed.

2. Experimental Section

2-1. Transient Absorption Measurements. The transient absorption spectra were measured by a standard pump−probe technique using an amplified picosecond pulsed dye laser.[25] A pulse of a Nd:YAG laser (Coherent Antares 76-S)-pumped dye laser (Coherent 700; $\lambda = 590$ nm), which was amplified with a dye amplifier system (Continuum PTA60 and Continuum RGA60) was split by a 50−50 beam splitter for the pump and probe beams. The laser power was ∼0.5 mJ/pulse at 50 Hz.

10.1021/jp991000s CCC: $18.00
Published on Web 11/05/1999

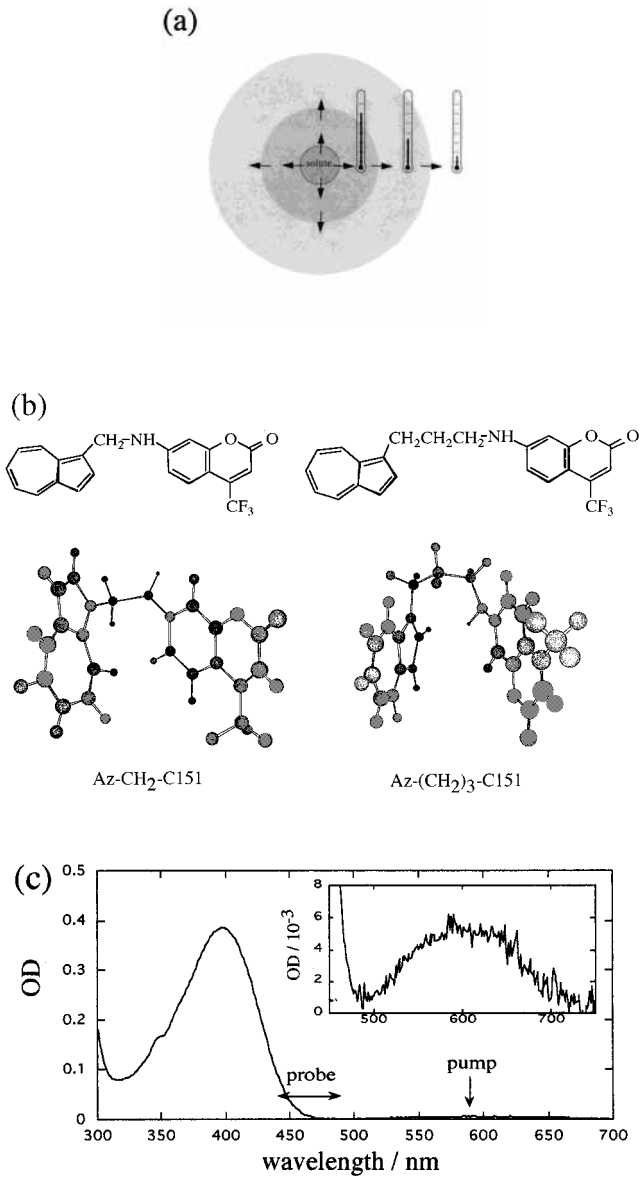

Figure 1. (a) Schematic showing how the transient temperature can be monitored with a high spatial resolution. (b) Optimized molecular structure of Az−CH_2−C151 and Az−$(CH_2)_3$−C151 by the semiempirical molecular orbital calculations (AM1 method). (c) Absorption spectrum of Az−CH_2−C151/ethanol.

The probe beam was focused by a lens ($f = 15$ cm) and brought into a 1 cm cell of flowing water to generate a white light continuum. The white light continuum then passed through a polarizer to select a vertically polarized light and was split into two (sample and reference beams) with a beam splitter. The sample beam was focused by a concave mirror ($R = 50$ cm) and brought into a sample cell. The optical path length was 3 mm. The pump beam was focused into the sample cell with a lens ($f = 50$ cm). The polarization of the pump beam was adjusted to the magic angle (54.7°). The probe beam after a sample cell and the reference beam were collected to an optical fiber connected to a spectrometer (Chromex 250IS) and detected by an intensified silicon photodiode array (EG&G, OMA1421). The signal was normalized by the reference, and the difference of the optical density (ΔOD) with and without pump beam was measured at each delay time. The system response curve was measured by the optical Kerr signal of the neat carbon tetrachloride solution under the same experimental conditions. The curve was fitted by a Gaussian function and the fwhm of the response was found to be typically 5 ps. The time origin ($t = 0$) was set at the peak of this cross correlation signal. The concentration of the sample was ∼5 mM in ethanol and 2-propanol for Az−CH_2−C151 and ∼10 mM in acetone and benzene for Az−CH_2−C151 and Az−$(CH_2)_3$−C151. The sample solution was photoexcited by the laser pulses with $\lambda =$ 590 nm. From the intensity of the pump pulse and the pumped area ($\sim 2 \times 10^{-3}$ cm), we calculated that ∼8% of the solute molecules were photoexcited in a typical case. All the solvents (ethanol, 2-propanol, acetone, benzene, and carbon tetrachloride (Nacalai Tesque, Spectral grade)) were used without further purification.

2-2. Steady-State Absorption Measurement under a Constant Density. The setup for the steady-state absorption measurement under a high-pressure condition is reported elsewhere.[26] Briefly, the absorption spectra were recorded with a spectrometer (Shimadzu UV-2500PC). A high-pressure optical cell was used at elevated pressures. The stability of the temperature was ±0.2 °C. The pressure was measured by a Heise Bourdon Tube gauge with a ±0.2 MPa accuracy. The densities of the solution were calculated from the *PVT* data of ethanol.[27]

3. Results

3-1. Az−CH_2−C151. The absorption spectrum of Az−CH_2−C151 (Figure 1c) is almost the same as the sum of the absorption spectra of azulene and of C151 except for slight red shifts (∼10 nm). Hence, the intermolecular interaction between azulene and C151 in the ground state appears to be weak. The absorption band from 500 to 700 nm is mainly the $S_0 \rightarrow S_1$ transition band of the azulene moiety and does not overlap with the long wavelength edge of the 0−0 transition of the C151 moiety. Therefore, we can photoexcite only azulene to the S_1 state using the laser light centered at 590 nm.

The observed transient absorption spectrum of Az−CH_2−C151/ethanol is shown in Figure 2a. The signal appears just on the red edge region of the C151 absorption band. The time evolution of the transient absorption signal probed at 450 nm is shown in Figure 2b. The time profile of the transient absorption signal is almost identical at all the wavelengths in which the transient absorption signal appears. The transient absorption spectra were also measured in acetone (Figure 3), 2-propanol, and benzene (Figure 4). The spectra are very much similar.

Previously, this signal was attributed to the hot band of the C151 absorption on the basis of the following reasons.[24] First of all, no signal was observed from the sample that contained only azulene or C151 under the same experimental conditions. Hence the observed transient absorption signal is not the absorption of the excited states of azulene or C151. Second, the wavelength in which the transient signal appears is on the red edge of the absorption band of C151. It could be possible that the signals come from the hot band of azulene. However, this contribution may be minor because the absorption coefficient of azulene is much smaller than that of C151. Indeed, when the observed transient absorption signal is converted to the absorption coefficient (ϵ), the frequency dependence of ϵ shows the characteristic feature of the hot band of C151 (Figure 5).[24] Moreover, the wavelength region in which the transient absorption signal appears depends on the solvent, and this dependence can be reasonably explained by the solvatochromic shift of the C151 absorption band.[28] Therefore, we conclude that the observed transient absorption signal is due to the hot band signal of C151.

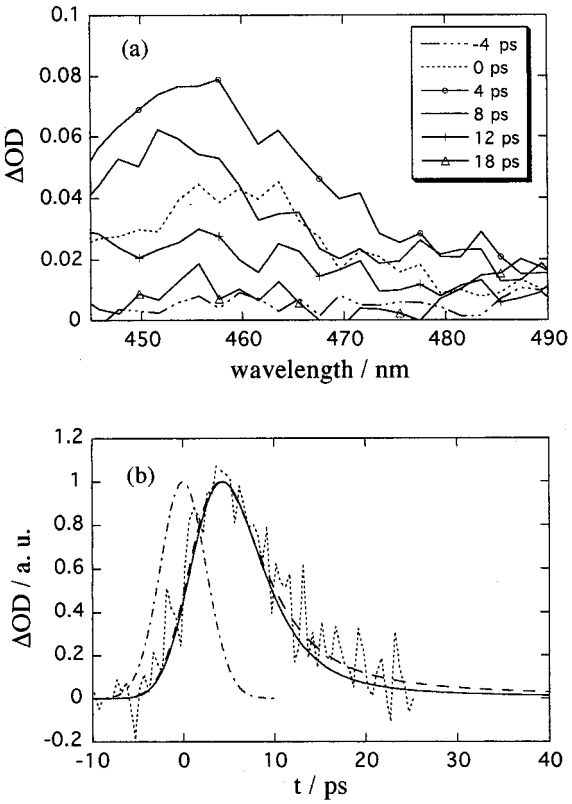

Figure 2. (a) Transient absorption spectrum of Az−CH_2−C151 in ethanol. (b) Time profile of the transient absorption signal probed at 450 nm (dotted line). The solid line represents the calculated signal based on the thermalization model with the IVR process ($\tau_{IVR} = 5$ ps and $\tau = 3$ ps). The system response curve is represented by the point-dashed line. The fitted curve with the second thermalization model (without the IVR process) is also shown by the broken line ($\tau_{sum} = 3$ ps).

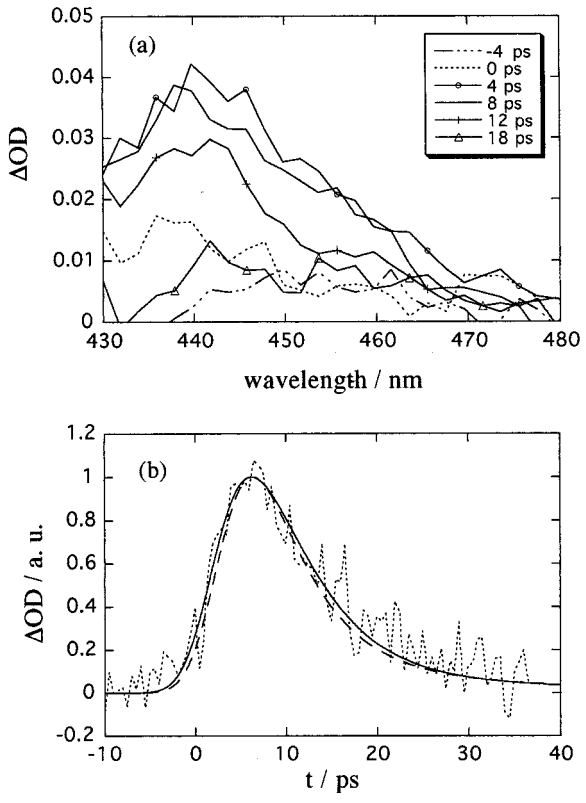

Figure 3. (a) Transient absorption spectrum of Az−CH_2−C151 in acetone. (b) Time profile of the transient absorption signal probed at 440 nm (dotted line). The solid line represents the calculated signal based on the thermalization model with the IVR process ($\tau_{IVR} = 30$ ps and $\tau = 4$ ps). The fitted curve with the second thermalization model (without the IVR process) is also shown by the broken line ($\tau_{sum} = 7$ ps).

Besides the hot band signal, when the excitation laser power was strong, another component of the transient absorption signal was observed in a longer wavelength region. This component is particularly clear in benzene at a wavelength around 455 nm (Figure 4). This signal quickly rises, and the decay is very fast (<1 ps). The time profile of this component is about the same as the instrumental response function. The origin of this component is not clear at present but could be a transient absorption from higher excited states produced by the multiphoton absorption. This contribution can be minimized by using a weak pump laser power. This component is not seen in the signals of the ethanol, 2-propanol, and acetone solutions. The amplitudes of the hot band signals were proportional to the pump laser power. Hence we believe that this contribution does not participate in the hot band signals we are studying.

3-2. Az−$(CH_2)_3$−C151. The hot band spectrum of Az−$(CH_2)_3$−C151 in acetone is shown in Figure 6a. The fast rising signal observed in Az−CH_2−C151/benzene was also observed in this system when the pump laser power was strong. The spectrum of this component was estimated from the transient absorption spectra of Az−CH_2−C151 in acetone recorded at a stronger pump laser power. The hot band spectrum (Figure 6a) is obtained by subtracting the estimated spectrum of this component from the raw data. The time profile of the transient absorption signal probed at 450 nm is shown in Figure 6b. The time evolution of this signal is very similar to that of Az−CH_2−C151 except for the long time behavior and a weaker intensity.

The transient absorption signal was observed also in benzene. The spectrum and the time profile of the signal are similar to those of Az−CH_2−C151 in benzene. We could not observe any signal in ethanol and 2-propanol because of the low solubilities of Az−$(CH_2)_3$−C151.

4. Discussion

4-1. Analysis of the Transient Temperature. A simple interpretation of the observed transient spectra is that the signal directly reflects the temperature rise of C151 due to the thermal energy dissipation from azulene. However, we must consider that the absorption coefficient (ϵ) is not generally proportional to the temperature. First, we examine the relationship between ϵ and T at the probe wavelength. The hot band absorption appears due to the thermal excitation of higher vibrational levels in the ground state. Kaiser and co-workers introduced the following model for analyzing the temperature-dependent electronic absorption spectrum, which has been used in many systems.[1,29−31] In this model, ϵ at a wavenumber ν and at a temperature T is expressed by

$$\epsilon(\nu,T) \propto S(\nu) \exp\{-h(\nu - \nu_{00})/kT\} \quad (1)$$

where ν_{00} is the wavenumber of the 0−0 transition and k is the Boltzmann constant. $S(\nu)$ is determined by the density of the vibrational states and the Franck−Condon factors. If we assume that the temperature dependence of ϵ is expressed by eq 1, the ratio of $\epsilon(\nu,T)$ to that at room temperature ($T_{rt} = 298$ K) is given by

$$\frac{\epsilon(\nu,T)}{\epsilon(\nu,T_{rt})} = \exp\{h(\nu - \nu_{00})(1/kT - 1/kT_{rt})\} \quad (2)$$

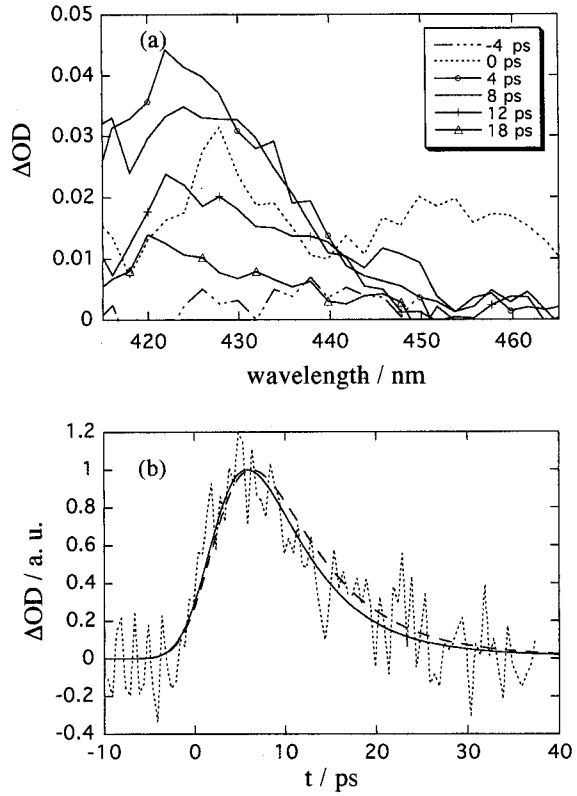

Figure 4. (a) Transient absorption spectrum of Az−CH_2−C151 in benzene. (b) Time profile of the transient absorption signal probed at 420 nm (dotted line). The solid line represents the calculated signal based on the thermalization model with the IVR process ($\tau_{IVR} = 10$ ps and $\tau = 5$ ps). For comparison, the calculated signal with $\tau_{IVR} = 10$ ps and $\tau = 6$ ps is also represented by the broken line.

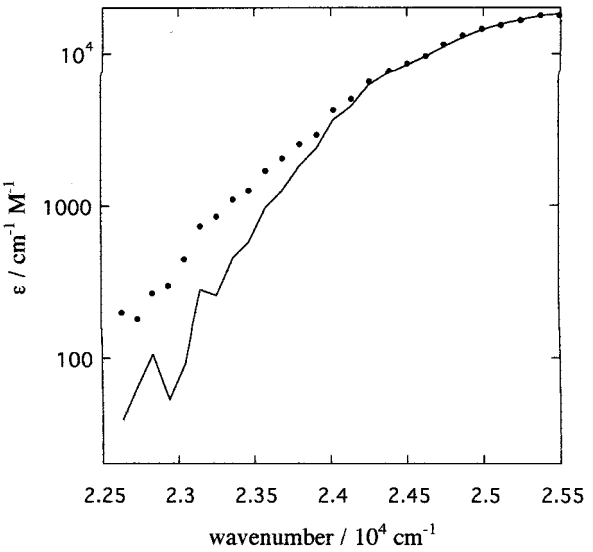

Figure 5. Red edge of the C151 absorption spectrum at room temperature (solid line) and absorption coefficient at 5 ps after photoexcitation of azulene moiety in benzene (circles).

Let us examine eq 2 for the transient absorption signal of Az−CH_2−C151/ethanol. The ratio of $\epsilon(T)$ measured at 4 ps after photoexcitation to $\epsilon(T_{rt})$ is shown in Figure 7a. If the above analysis is appropriate, the plot of $\ln\{\epsilon(T)/\epsilon(T_{rt})\}$ vs ν should be linear. However, the plot deviates from the linear relation at a higher wavenumber region. Probably this deviation is due to the contributions from the vibronic bands in the excited state. We fitted the data points in the red edge region by a linear function of ν with a parameter of ν_{00} and T (solid line in Figure

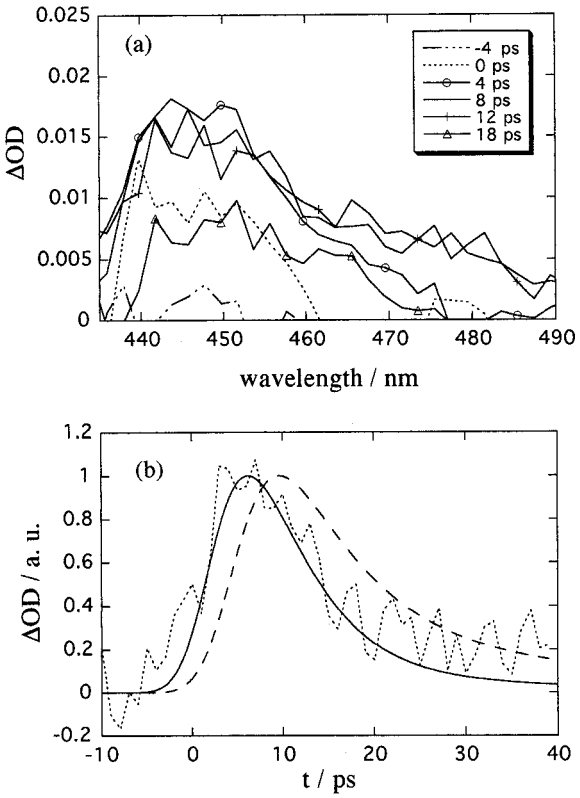

Figure 6. (a) Transient absorption spectrum of Az−$(CH_2)_3$−C151 in acetone. (b) Time profile of the transient absorption signal probed at 450 nm (dotted line). The solid lines represent the same calculated signal as in Figure 2b. The broken line denotes the time profile of the transient temperature of the thermometer calculated with the second thermalization model ($\tau_{sum} = 7$ ps) when the propylene chain is stretched out (the distance between the heater and thermometer is ∼11 Å).

7a). From the fitting, we determined $\Delta T = T - T_{rt} \approx 66$ K and $\nu_{00} = 22\,400$ cm^{-1}. The uncertainty of the temperature is estimated to be ±10 K from a different set of the fitting with different wavelength regions and also from several runs of the experiments. The frequency of the 0−0 transition is reasonably close to that estimated from the absorption and the fluorescence spectra of Az−CH_2−C151/ethanol (22 500 cm^{-1}). This agreement supports the validity of this estimation and our interpretation that the induced absorption in this region comes from the thermal broadening of the 0−0 transition band of C151.

By using the determined ν_{00} (=22 400 cm^{-1}), the temperature dependence of $\epsilon(T)$ at the probe wavelength of 450 nm can be calculated from eq 1 (Figure 7b). The plot of ϵ vs T shows that ϵ is almost proportional to T in this temperature range. Therefore, we conclude that the observed transient absorption signal intensity at 450 nm is directly proportional to the temperature change of the molecular thermometer. In the other solvents used here, this linear relationship is valid, too. On the basis of these results, hereafter, we analyze the temperature change of the molecular thermometer (C151) from the time profile of the transient absorption signal.

To calibrate the temperature rise from the transient absorption intensity by another method, the temperature dependence of the steady-state absorption spectra of Az−CH_2−C151 was measured at several temperatures under ambient pressure. Generally, with increasing temperature, the absorption spectrum is thermally broadened due to the population increase of the higher vibrational levels. The observed $S_0 \rightarrow S_1$ absorption band of C151 at higher temperature is thermally broadened, as expected. However the entire absorption band shifts to the blue side with

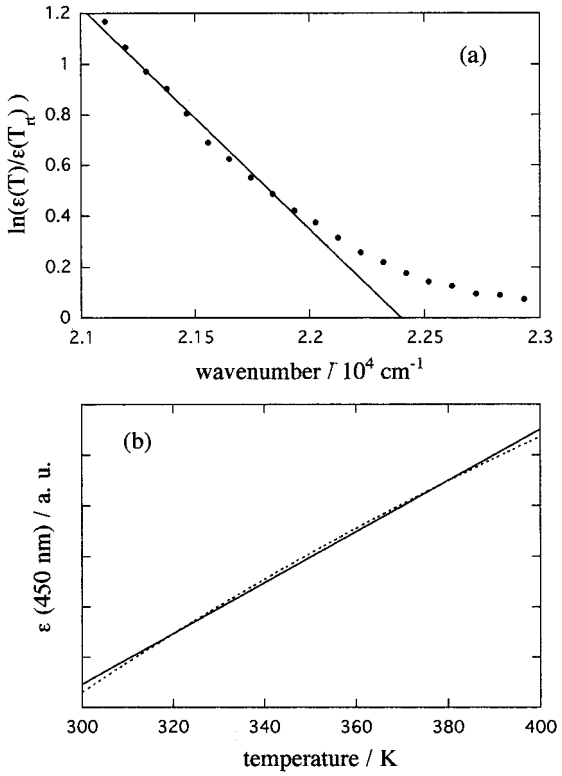

Figure 7. (a) Ratio of $\epsilon(T)$ at 4 ps after the photoexcitation to $\epsilon(T_{rt})$ of Az−CH_2−C151/ethanol. The solid line denotes the fitting line by using eq 2. (b) Relation between the absorption coefficient at 450 nm (ϵ(450 nm)) and the temperature (dotted line). The solid line denotes the best fitted line by a linear function.

increasing temperature, and the hot band did not appear in the red edge. This was totally unexpected. This spectral shift at a higher temperature, however, has been observed for many molecules and is known as "thermochromism".[32,33] This observation is inconsistent with the hot band observation in the transient absorption spectrum.

A similar phenomenon in studies of the transient temperature has been sometimes reported so far. For example, Scherer et al. tried to calibrate the transient temperature of the molecular thermometer (oxazine-1) in a picosecond time scale by using the steady-state absorption spectrum.[34] In this case, the hot band signal could be fitted not by a spectrum expected at a high temperature but by a spectrum after a correction for the thermochromic shift. In their analysis, the origins of the temperature dependence of the steady-state spectrum were divided into three components: the first, the absorption change of optically active modes with large Franck−Condon factors induced by the increase in thermal population, the second, the line broadening due to the population change of low-frequency modes and the modes with small Franck−Condon factors, and the third, the temperature-dependent shift of the absorption spectrum. They found that the observed transient spectrum should be fitted by the first two components. They concluded that the steady-state absorption spectrum cannot be compared with the transient absorption spectrum in a picosecond time scale probably because the thermochromic shift takes place slowly by the change of the dielectric constant and the refractive index of the solvent.

The thermochromism results from the temperature dependence of the orientational and the isotropic polarization of the solvent.[32,33] The time responses of these contributions are unclear because systematic time-resolved studies of the thermochromism are quite limited. The orientational response of the solvent may

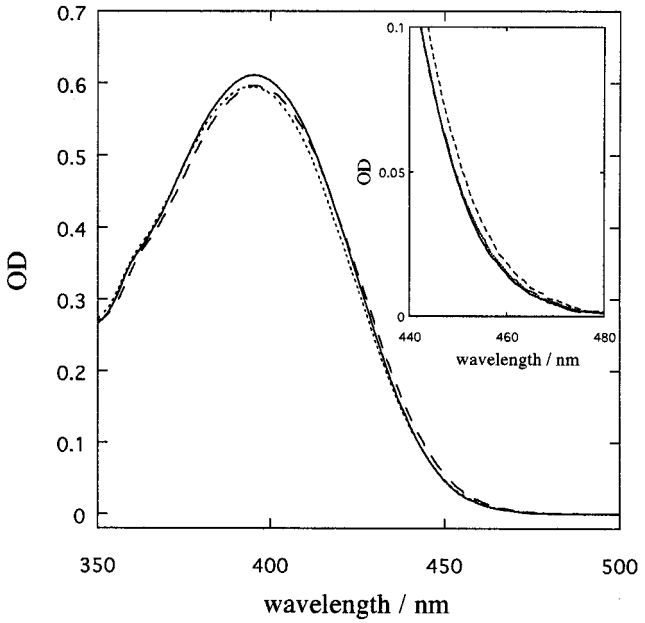

Figure 8. Absorption spectrum of C151 in ethanol under $\rho = 0.81$ g cm^{-3}. The solid and dotted lines denote the observed spectra at 25 and 50 °C, respectively. The spectrum corrected for the thermochromism is shown by the broken line.

be very fast because a large part of the dynamic Stokes shift occurs in the very short time scale, which is induced by the oriental redistribution of the surrounding solvents.[35−40] On the other hand, the temperature dependence of the isotropic contribution comes from the density variation, which could take place slowly. We measured the absorption spectrum at a constant density (ρ) to subtract the isotropic contribution. The temperature dependence of the absorption coefficient $\Delta\epsilon/\Delta T$ was determined from the absorption spectrum of Az−CH_2−C151 in ethanol under $\rho = 0.81$ g cm^{-3} at 25 °C and 50 °C (Figure 8). Assuming $\Delta\epsilon \propto \Delta T$, $\Delta\epsilon/\Delta T$ was found to be 1.7 cm^{-1} M^{-1} K^{-1} at 455 nm in ethanol. By using this value, a temperature rise of ∼290 K at the maximum is calculated from the transient absorption intensity of Az−CH_2−C151/ethanol. This temperature rise of ∼290 K is inconsistent with the estimated ΔT from the red-edge analysis of the absorption spectrum presented before (∼66 K).

Next we subtract the temperature-dependent blue shift from the observed temperature dependence of the absorption spectrum; that is, the observed absorption spectrum at 50 °C is shifted so that the peak of the absorption spectrum at 50 °C matches that at 25 °C (broken line in Figure 8). If we use this spectral correction, $\Delta\epsilon/\Delta T = 6.4$ cm^{-1} M^{-1} K^{-1} is obtained at 455 nm, which leads to $\Delta T - 78$ K at the peak of the transient absorption intensity. It is rather surprising that this temperature rise is within the uncertainty range of the estimated ΔT from the analysis of the red edge broadening of the absorption spectrum. This coincidence may indicate that the absorption spectrum shift due to the temperature rise occurs slowly, and the transient broadening should be analyzed without taking into account the frequency shift of the spectrum. However, the detailed mechanism about the thermochromism including its time response is still unclear, and further studies are needed to reveal the relationship between the transient and the steady-state absorption spectra.

4-2. Theoretical Models of the Thermalization Process. The hot band absorption appears because the vibrational levels of the thermometer are thermally excited. In the present case, there are two possible energy transfer mechanisms: through-

bond and through-solvent mechanisms. The former process can be regarded as an intramolecular vibrational redistribution (IVR) process of the azulene-coumarin integrated molecule.

First, we tried to reproduce the observed temporal profile of the temperature and the temperature increase (ΔT) using a simple thermalization model, which includes the IVR process and through-solvent energy transfer. We assumed that the excess energy of the photoexcited azulene is transferred to the thermometer (C151) through the σ-bond with a lifetime of τ_{IVR} as well as through several effectively coupled solvent molecules (directly energy accepting (DEA) solvent molecules) with a lifetime of τ. The DEA solvents should locate in the first solvent shell of the azulene−coumarin integrated molecule. We also assumed that the energy transfer rate is proportional to the temperature difference between the energy donor and acceptor molecules. The internal excess energy of azulene increases with two steps: $S_1^* \rightarrow S_1$ (S_1^*: the Franck−Condon state from the ground state) and $S_1 \rightarrow S_0$ processes (1 ps). Since the $S_1^* \rightarrow S_1$ process of azulene is completed very quickly (less than 1 ps),[16] the time evolution of the solute energy from this process can be neglected. This contribution provides an initial condition of the azulene temperature; $T_A(t=0) = Q_0/C_{Az}$ ($Q_0 = h\nu - E(S_1)$ and C_{Az} is the heat capacity of azulene). T_{Az} is further elevated by the energy from the deactivation of the S_1 state with a lifetime of τ_{S1} (=1 ps). Therefore, the time evolution of the temperature of azulene can be given by

$$C_{Az}\frac{dT_{Az}(t)}{dt} = C_{Az}\left(-\frac{T_{Az}(t) - T_{C151}(t)}{\tau_{IVR}}\right) + C_{Az}\left(-\frac{T_{Az}(t) - T_{DEA}(t)}{\tau}\right) + \frac{E(S_1)}{\tau_{s_1}}\exp(-t/\tau_{s_1}) \quad (3)$$

where T_{C151} and T_{DEA} are the temperatures of C151 and the DEA solvents, respectively.

The thermometer C151 receives the excess energy from azulene directly and dissipates (or accepts) the energy to (or from) the DEA solvents. We assumed that the rate constant of the intermolecular energy transfer between C151 and the DEA solvent is the same as that between azulene and the DEA solvent (τ^{-1}). Hence, the temperature changes of C151 and the DEA solvents are given by

$$C_{C151}\frac{dT_{C151}(t)}{dt} = C_{Az}\left(\frac{T_{Az}(t) - T_{C151}(t)}{\tau_{IVR}}\right) + C_{C151}\left(-\frac{T_{C151}(t) - T_{DEA}(t)}{\tau}\right) \quad (4)$$

$$N_{DEA}C_{solv}\frac{dT_{DEA}(t)}{dt} = C_{Az}\left(\frac{T_{Az}(t) - T_{DEA}(t)}{\tau}\right) + C_{C151}\left(\frac{T_{C151}(t) - T_{DEA}(t)}{\tau}\right) \quad (5)$$

where C_{C151} and C_{solv} are the heat capacities of C151 and the solvents, respectively. N_{DEA} is the number of the DEA solvents.

The thermal energy of the DEA solvent diffuses to the outer solvents (which is assumed to be continuous) by the thermal diffusion. The thermal diffusion process to the outer sphere under the spherical symmetry condition may be described by[41]

$$\frac{\partial(rT(t))}{\partial t} = D\frac{\partial^2(rT(t))}{\partial r^2} \quad (6)$$

TABLE 1: ΔT Obtained by the Simple Estimation with Eqs 1 and 2, the Obtained τ_{IVR} and τ by the Curve Fitting with the First Thermalization Model, τ_{Sum} To Reproduce the Observed Time Profile of the Hot Band Signal with the Second Thermalization Model, and the Parameters Used in the Calculations

	ethanol	2-propanol	acetone	benzene
ΔT/K	66	17	37	68
τ_{IVR}/ps	5 ± 2	20 ± 10	30 ± 10	10 ± 5
τ/ps[a]	3	2	4	5
τ_{sum}/ps[b]	3	3	7	5
$C_{solvent}$/J K^{-1} mol^{-1}	112	157	136	126
L/Å	4	4.5	4	5.5
D/10^{-8} m^2 s^{-1}	8.6	6.9	9.3	9.4

[a] Uncertainty of τ is ±1 ps. [b] Uncertainty of τ_{sum} is ±2 ps.

where T is the temperature of the bulk solvent, r is the distance from the center of the heater, and D is the thermal diffusivity.

The S_1-S_0 energy spacing ($E(S_1)$) is estimated to be ~14 500 cm^{-1}.[8,16] The heat capacity (C_{solute} = 186 J mol^{-1} K^{-1}) of azulene were estimated from ref 7. The heat capacity of C151 was estimated from C_{C151}/C_{solv} obtained by a semiempirical molecular orbital calculation by the AM1 method with the MOPAC program package and the literature value of C_{solv}. N_{DEA} was determined from the estimated volume of the first solvent shell and the density of the solvent.[42] The radius of Az−CH$_2$−C151 was estimated to be 4 Å by using the method of atom increment.[43] The molecular size of the solvent (L) is calculated from the Lennard-Jones parameters.[44] The other parameters used in the calculation are listed in Table 1. These differential equations (3)−(6) are numerically solved.

By adjusting τ_{IVR} and τ, we tried to reproduce the time profile of the signal and the temperature rise (ΔT). We found that the temporal profile can be reproduced well by several sets of these parameters. For example, in the Az−CH$_2$−C151/ethanol case, the profile calculated with τ_{IVR} = 1 ps and τ = 6 ps is almost indistinguishable from that with τ_{IVR} = 5 ps and τ = 3 ps within the experimental uncertainty of the signal. However, if τ_{IVR} is as short as 1 ps, for example, the maximum temperature rise is 200 K, which is too high to explain the observed signal. Considering the experimental value (66 ± 10 K), we found that the signal can be reproduced well with τ_{IVR} = 5 ± 2 ps and τ = 3 ± 1 ps. The determined τ_{IVR} and τ in the other solvents are summarized in Table 1, and the calculated signals are depicted in Figures 3, 4, and 6.

The obtained τ_{IVR} and τ indicate some characteristic features. (1) Although the IVR of large molecules in solution is believed to occur within a few picoseconds, the observed τ_{IVR} are rather long. As stated above, the temporal profile can be also reproduced with τ_{IVR} = 1 ps and τ = 6 ps, but it gives too high of a temperature rise. τ_{IVR} have to be longer than 3 ps in ethanol and 20 ps in acetone to explain the temperature rise. The slow τ_{IVR} will be discussed later in this section. (2) These τ_{IVR} strongly depend on the solvent. Since the IVR process of many large molecules usually completes within an experimental time resolution, systematic studies on the solvent dependence of the IVR process are highly limited and the detailed mechanism is still unclear. The present results mean that the slow IVR process may be sensitive to the solute−solvent interaction. Further information is needed to reveal the solvent dependence of the IVR process. (3) The obtained τ are shorter than the previously reported vibrational cooling times of azulene.[6,7,9] The thermalization times of some other molecules were also found to be faster than 5 ps.[21−23] This shorter τ will be also discussed in the later part of this section.

Besides the above three features, it is worthwhile to point out that the obtained τ_{IVR} are much longer than τ. For the

purpose of comparison, we constructed another thermalization model, in which the energy transfer through the σ-bond is neglected. This second model allows us to calculate the transient temperature of the molecular thermometer at various distances from the molecular heater.

First, the temperature of solvent is calculated and then the temperature of the molecular thermometer at a distance from the excited solute is calculated. The first step of the calculation is similar to the previous one. We calculated the energy dissipation process from azulene to solvent using eqs 3, 5, and 6 with negligible τ_{IVR} and without the molecular thermometer. The activation and the deactivation processes of the molecular thermometer (C151) were individually expressed as a response function. The response time of the temperature elevation and the temperature decrease of C151 could be different. However, using two different response times adds a complexity and more parameters to the model, and we will not gain much insight into the thermalization process. Hence we assume that the rate constants of the energy transfer to C151 and from C151 are identical ($1/\tau_{vib}$). Under this assumption, the response function of C151 ($g(t)$) after impulsive heating is given by

$$g(t) = \frac{t}{\tau_{vib}} \exp(-t/\tau_{vib}) \tag{7}$$

As regarding the distance between the heater and the thermometer, we should take a distance between a point where the energy is released and a point where the temperature is detected in the molecular structures. However, we do not know which part of azulene releases the heat and which part of C151 is sensitive to the temperature. Hence we take the center-to-center distance between the chromophores to represent the distance between the heater and the thermometer, which is estimated to be 0.65 nm from the optimized geometry (Figure 1b) by a semiempirical molecular orbital calculation (AM1 method, MOPAC program package). The radius of azulene is 0.33 nm,[7] and the diameters of the solvents used here are 0.43−0.55 nm.[44] We assume that the molecular thermometer locates between the DEA solvents and the outer continuum medium. The temperature of C151 increases by the energy flow from the DEA solvents and decreases by the energy transfer to the continuum. Therefore, the experimentally observed $\Delta T_{C151}(t)$ is expressed by

$$\Delta T_{C151}(t) = \int_{-\infty}^{t} \Delta T_{DEA}(t - t')\, g(t')\, dt' \tag{8}$$

Even using this simple model, the energy transfer rate from azulene to solvent ($1/\tau$) and the thermal excitation rate of C151 ($1/\tau_{vib}$) could not be determined independently by the fitting of the observed transient temperature under our signal-to-noise ratio. After calculating the temporal profile of the transient temperature of C151 using various parameters, we found that the profiles calculated with the same $\tau_{sum} = \tau + 2.5\tau_{vib}$ give very similar curves. Hence we can determine only τ_{sum} from the fitting of the observed profile.

The best fit of the observed profile was obtained with $\tau_{sum} = 3$ ps in ethanol ($N_{DEA} = 16$). However, the calculated temperature rise is ~10 K, which is much lower than the observed rise. We may be able to improve the fitting two ways. First, a slight contribution of the IVR process could increase the temperature. A model taking into account of the IVR process is the first model we presented above in this section. Second, the higher temperature rise could be explained by a smaller N_{DEA} or smaller heat capacity of the solvent. If we fitted the time profile with $N_{DEA} = 2$, ΔT was found to increase ~30 K, which was closer to the experimental value (66 ± 10 K). A possibility of the smaller N_{DEA} may suggest that the energy transfer to the solvent is selective to a few DEA solvent molecules. The mechanism of the selective thermal energy transfer to some DEA solvents was used previously to explain the thermalization rate of 2-hydroxybenzophenone.[23] Also it is consistent with theoretical studies by Nagaoka et al.[45] and the experimental finding that the thermalization is significantly enhanced by a specific intermolecular interaction such as the hydrogen bonding.[22] The calculated curves (after normalized to the peak intensity of the observed signals) are shown in Figures 2 and 3 as examples. The obtained τ_{sum} with $N_{DEA} = 2$ are listed in Table 1. A possibility of the small C_{solv} for the transient temperature was discussed in the previous paper,[23] and we think it is conceivable in this case, too.

From these two model calculations, we found that the observed transient temperature can be explained by the thermalization model with the IVR process or the model without IVR but with small N_{DEA} or small C_{solv}. At present, we do not know which model is more appropriate for describing the thermalization of this system. There are some drawbacks in both models. In the first model, the solvent-dependent IVR process is hard to explain. Furthermore, if the IVR process through the σ-bond is important, the time profile of the transient temperature of the longer chain molecule, Az−$(CH_2)_3$−C151, is expected to be different from Az−CH_2−C151, but it is not observed here. In the second model, the origin of the small N_{DEA} or C_{solv} is not clear. This point should be clarified for the thermalization study by the molecular heater−molecular thermometer system in the future.

It is important to stress that, by using either models, the thermalization process of Az−CH_2−C151 must be fast to explain the observations; that is, the excess energy of azulene efficiently transfers to C151 through the solvent. The determined thermalization times (τ or τ_{sum}) are shorter than the vibrational relaxation time obtained by monitoring the vibrational temperature of azulene itself.[7,9] What is the origin of the difference between the thermalization times determined here and those reported previously? We may think the following two possibilities. First, combining the methylene group and C151 should increase the density of states around azulene. As a result, the coupling between the vibrational modes of azulene and the translational mode of the DEA solvents becomes strong and the cooling time of azulene could be faster than the isolated azulene case. Second, the nonuniform intramolecular vibrational relaxation may participate in the difference. If the intramolecular vibrational redistribution is fast enough compared with the vibrational cooling process, the temperature decrease monitored from the solute temperature should be the same as the temperature increase monitored outside of the solute. However, if the intramolecular vibrational relaxation is not fast enough compared with the thermalization process, we should observe several kinetics in the thermalization process. For example, it could be possible that the hot band detection method in the previous studies monitored the populations of the vibrational levels with low vibrational quantum numbers, while the transient temperature detection in this study monitors overall energy transfer from azulene to the solvent. If most of the vibrational populations dissipate their excess energy to the solvents very quickly, the temperature of the solvent rises very fast and the minor part of the temperature rise could not be detected. On the other hand, the hot band detection of azulene is sensitive to the population dynamics of the vibrational levels with relatively large Franck−

Condon factors in the S_1 state and the relaxation of these states could be slow.

A typical time scale of the intramolecular vibrational relaxation has been believed to be in the range of subpicoseconds for large molecules.[1] If this is the case for azulene, the second explanation is unrealistic. Recently, however, slow intramolecular relaxation processes (several picoseconds) have been observed in several large molecules.[46−51] For example, Nakabayashi et al. studied the intramolecular vibrational relaxation of *trans*-stilbene by picosecond time-resolved anti-Stokes Raman spectroscopy.[51] They found that the intramolecular vibrational relaxation process proceeds in roughly two steps. Although the highly excited vibrational levels of the olefinic stretching modes relax very rapidly (in the femtosecond to subpicosecond time range), the nonequilibrium S_1 state persists for several picoseconds after photoexcitation. Therefore, not only IVR between azulene and C151 moieties but also the intramolecular vibrational relaxation time of azulene may be in the several picosecond time scale. Schwarzer et al. considered that 3 ps may be a reasonable intramolecular relaxation time for azulene when they found that the cooling rates deviated from the isolated binary collision model in a higher density region.[9] To clarify the existence of the fast energy dissipation process, a photothermal spectroscopic study on the vibrational cooling of azulene is required.

The determined thermalization times (τ and τ_{sum} in Table 1) depend on the solvent. The thermalization occurs faster in the alcoholic solution. We believe that the short thermalization time in the alcoholic solvent is due to the hydrogen bonding between azulene and the solvent. It was already reported that the hydrogen bond formation has a strong influence on the vibrational cooling rate of azulene.[9] The same tendency has been reported in other systems.[18,22,52,53] Recently, McDowell studied the collisional deactivation of the triplet pyrazine in the gas phase.[52] They found that water is an unusually strong vibrational relaxer. Terazima reported that the thermalization rate of Betaine-30 has a good correlation with the hydrogen bond density.[22] The thermalization time in a mixture of water and ethanol becomes shorter with the increasing mole fraction of water. The importance of the hydrogen bonding was suggested theoretically by the molecular dynamics simulation, too.[53]

4-3. Az−$(CH_2)_3$−C151. The time profile of the transient absorption of Az−$(CH_2)_3$−C151 (Figure 6b) is very similar to that of Az−CH_2−C151 except for the signal intensity. Naturally, the profile can be fitted by the same model presented for Az−CH_2−C151 (solid line in Figure 6b). If the propylene chain is stretched out, the distance between azulene and C151 is estimated to be ∼11 Å from the semiempirical molecular orbital calculation. In this case, the calculated time profile with the second thermalization model is clearly delayed and does not reproduce the observed signal (broken line in Figure 6b). This result indicates that the C151 moiety should locate near the azulene moiety due to the flexibility of the propylene chain. One of notable differences is that the signal intensity of Az−$(CH_2)_3$−C151 is ∼3 times weaker than that of Az−CH_2−C151. The weaker intensity may come from two factors. First, the distance between azulene and C151 could be rather broadly distributed. From the signal intensity, we think that about one-third of C151 locates in the vicinity of azulene. It was reported that the chromophores connected with a flexible spacer can be close to each other.[54−57] Second, since the thermal energy is conducted uniformly in space, the temperature rise at a far distance from the molecular heater should be smaller than that at a closer distance. Hence, the compound that has a long distance between azulene and C151 cannot contribute to the transient temperature signal significantly. We think that these two factors make the time profile of the transient temperature of Az−$(CH_2)_3$−C151 similar to that of Az−CH_2−C151.

It may be interesting to note that the deviation of the calculated temperature rise from the observed signal can be seen in the long time delay. This feature was always observed also in benzene although the signal-to-noise ratio is not good. This long tail may represent the time development of the temperature at the outer sphere, which was monitored by the lengthened form of Az−$(CH_2)_3$−C151. It may be very interesting to study the transient temperature from compounds with a rigid spacer between the two chromophores to fix the distance between the heater and the thermometer. Such molecular integrated systems will provide ideal systems for revealing the thermalization process with a high spatial resolution. A study along this line will be conducted by this group in the future.

5. Conclusion

A very fast vibrational cooling process of azulene was studied by the transient absorption method using molecular integrated systems with a molecular thermometer (C151). Vibrationally highly excited azulene (molecular heater) is formed by the light absorption into the S_1 state and the subsequent relaxation to the ground state by the internal conversion with a lifetime of 1 ps. After the azulene moiety was photoexcited, the transient absorption signal was observed at the red edge of the $S_0 \rightarrow S_1$ absorption band of the C151 moiety. First, a compound combined with the methylene chain between the heater and the thermometer (Az−CH_2−C151) was examined. The observations were analyzed with the thermalization model, which includes the through-bond and the through-solvent energy transfer. From this analysis, it was found that the energy transfer times by the IVR process are in a range of 5−30 ps depending on the solvents, and the cooling times of azulene were less than 5 ps. The time profiles of the transient temperature can be also reproduced by another thermalization model without the IVR process, but in this case, we have to assume that the number of the DEA solvent is smaller than the number of the solvent molecules in the first solvent shell or C_{solv} is smaller than that under the steady-state conditions. The thermalization time determined by this model is also short (<7 ps). These results indicate that there is a very fast thermalization process of hot azulene compared with that reported from the hot band detection of azulene itself. This vibrational cooling rate depends on the solvent. The transient absorption spectrum and the time profile of a compound with a longer chain (Az−$(CH_2)_3$−C151) are very similar to those of Az−CH_2−C151 except for the signal intensity. This fact indicates that about one-third of the C151 moiety locates in the vicinity of azulene moiety because of the flexibility of the propylene chain. The deviation from the calculated signal was observed in the long time delay, which may reflect the temperature of the solvent in the outer shell.

6. Synthesis

All ^{1}H NMR spectra were recorded on a JEOL alpha-500 (operating at 500 MHz), and FAB-MS spectra were recorded on a JEOL HX-110 with a 3-nitrobenzyl alcohol matrix. Azulene (Lancaster) and C151 (SIGMA) were used as received.

6-1. Az-CH_2−C151. *7-((Azulen-1-yl)methylideneamino)-4-trifluoromethylcoumarin (Az−CH═C151).* A 50 mL flask equipped with a Dean−Stark trap, a magnetic stirrer, and a reflux condenser was charged with 0.458 g (2 mmol) of 7-amino-4-trifluoromethylcoumarin (C151), 1-azulenecarbox-

aldehyde (0.312 g, 2 mmol), *p*-toluenesulfonic acid (0.0380 g, 0.2 mmol), and toluene (25 mL). 1-Azulenecarboxaldehyde was prepared from azulene by the previously reported method.[58] This mixture was heated to reflux in an oil bath under nitrogen with stirring for 2 days. The mixture was cooled to room temperature, and the orange-red solid was collected by filtration. The solid was washed twice with benzene and dried in vacuo to give 0.530 g (1.4 mmol, 70%) of pure Az−CH═C151. ^{1}H NMR (δ in $CDCl_3$): 9.49 (d, 1H, J = 9.5 Hz, azulene ring), 8.99 (s, 1H, −CH═N−), 8.47 (d, 1H, J = 9.5 Hz, azulene ring), 8.34 (d, 1H, J = 4.0 Hz, azulene ring), 7.82 (t, 1H, J = 9.8 Hz, azulene ring), 7.75 (dd, 1H, J = 8.5 Hz, 1.3 Hz, coumarin ring), 7.55 (t, 1H, J = 9.8 Hz, azulene ring), 7.46 (t, 1H, J = 10 Hz, azulene ring), 7.44 (d, 1H, J = 4.5 Hz, azulene ring), 7.29 (d, 1H, J = 8.5 Hz, coumarin ring), 7.28 (d, 1H, J = 9.0 Hz, coumarin ring), 6.72 (s, 1H, coumarin ring). Mass spectrum: 368 (calcd for M + H$^+$: 368).

7-((Azulen-1-yl)methylamino)-4-trifluoromethylcoumarin (Az−CH_2−C151). Az−CH═C151 (0.25 g, 0.7 mmol) was dissolved in 10 mL of ethanol, and sodium borohydride (0.0265 g, 0.7 mmol) was added to the solution. In the dark, the solution was stirred for 2 days at room temperature under nitrogen. Water (∼0.5 mL) was added to the reaction mixture, which was allowed to stand for ∼5 min and then evaporated. The crude product was dissolved in 20 mL of benzene, and the dark purple solid was removed by filtration. The filtrate was chromatographed first on alumina (Sumitomo Kagaku KCG-1525, 2 cm in diameter and 3 cm height) with 1% methanol/benzene (v/v) and then on a size-extrication column (Biorad BIO-BEANS S-X1, 5 cm diameter and 50 cm height) with benzene. The first green fraction was collected and evaporated, to yield 0.0574 g (0.16 mmol, 22%) of Az−CH_2−C151. ^{1}H NMR (δ in $CDCl_3$): 8.37 (d, 2H, J = 9.5 Hz, azulene ring), 7.92 (d, 1H, J = 3.5 Hz, azulene ring), 7.67 (t, 1H, J = 9.8 Hz, azulene ring), 7.49 (dd, 1H, J = 8.5 Hz, 2.0 Hz, coumarin ring), 7.37 (t, 1H, J = 4.5 Hz, azulene ring), 7.24 (td, 1H, J = 10 Hz, 2.0 Hz, azulene ring), 6.61 (m, 2H, coumarin ring), 6.44 (s, 1H, coumarin ring), 4.83 (d, 2H, J = 4.0 Hz, −CH_2−), 4.64 (s, 1H, −NH−). Mass spectrum: 370 (calcd for M + H$^+$: 370).

6-2. Az−$(CH_2)_3$−C151. *Ethyl 3-(Azulen-1-yl)-2-propenoate (Az−CH═$CHCO_2C_2H_5$).* Triethyl phosphonoacetate (0.432 g, 1.92 mmol) was dissolved in 3 mL of benzene, and the solution was slowly added to sodium hydride (60% oil suspension) (0.0846 g, 2.12 mmol) under nitrogen. This mixture was stirred for 1 h. A solution of 1-azulenecarboxaldehyde (0.1 g, 0.641 mmol) in benzene (7 mL) was added under nitrogen, and the solution was heated to 60−65 °C with stirring for 5 h. The mixture was washed with water, extracted with benzene, and then evaporated. The resulting solid was chromatographed on silica gel with 10% ethyl acetate/hexane (v/v). The third dark blue fraction was collected and evaporated, to yield 0.111 g (0.491 mmol, 77%) of Az−CH═$CHCO_2C_2H_5$. ^{1}H NMR (δ in $CDCl_3$): 8.60 (d, 1H, J = 10.5 Hz, azulene ring), 8.32 (d, 1H, J = 15.5 Hz, −CH═), 8.31 (d, 1H, J = 10.5 Hz, azulene ring), 8.20 (d, 1H, J = 4.0 Hz, azulene ring), 7.67 (t, 1H, J = 10 Hz, azulene ring), 7.41 (d, 1H, J = 4.5 Hz, azulene ring), 7.32 (t, 1H, J = 10 Hz, azulene ring), 7.26 (t, 1H, J = 10 Hz, azulene ring), 6.47 (d, 1H, J = 15.5 Hz, ═CH−), 4.30 (q, 2H, J = 7.0 Hz, −CH_2−), 1.37 (t, 3H, J = 7.5 Hz, −CH_3).

Ethyl 3-(Azulen-1-yl)propanoate (Az−$CH_2CH_2CO_2C_2H_5$). A mixture of Az−CH═$CHCO_2C_2H_5$ (0.402 g, 1.78 mmol), nickel(II) chloride hexahydrate (0.127 g, 0.534 mmol), and sodium borohydride (0.404 g, 10.7 mmol) was dissolved in methanol (20 mL), and the solution was stirred under nitrogen for 2 h. The mixture was washed with water, extracted with dichloromethane, and then evaporated, to yield 0.333 g (1.46 mmol, 82%) of Az−$CH_2CH_2CO_2C_2H_5$. ^{1}H NMR (δ in $CDCl_3$): 8.31 (d, 1H, J = 9.5 Hz, azulene ring), 8.26 (d, 1H, J = 9 Hz, azulene ring), 7.79 (d, 1H, J = 4.0 Hz, azulene ring), 7.55 (t, 1H, J = 10.5 Hz, azulene ring), 7.33 (d, 1H, J = 4.0 Hz, azulene ring), 7.12 (t, 1H, J = 10 Hz, azulene ring), 7.09 (t, 1H, J = 9.5 Hz, azulene ring), 4.13 (q, 2H, J = 7.0 Hz, −CH_2−), 3.42 (t, 2H, J = 8.0 Hz, −CH_2−), 2.76 (t, 2H, J = 8.0 Hz, −CH_2−), 1.22 (t, 3H, J = 7.0 Hz, −CH_3).

3-(Azulen-1-yl)-1-propanol (Az−$(CH_2)_3OH$). Lithium aluminum hydride (0.222 g, 5.84 mmol) was added to a solution of Az−$CH_2CH_2CO_2C_2H_5$ (0.333 g, 1.46 mmol) in dry dimethyl ether (20 mL). The solution was immersed in an ice bath and stirred under nitrogen for 3 h. The mixture was washed with water, extracted with diethyl ether, and then evaporated. The resulting solid was chromatographed on silica gel with 50% ethyl acetate/hexane (v/v). The second blue fraction was collected and evaporated, to yield 0.0639 g (0.351 mmol, 24%) of Az−$(CH_2)_3$OH. ^{1}H NMR (δ in $CDCl_3$): 8.30 (d, 1H, J = 9 Hz, azulene ring), 8.25 (d, 1H, J = 9 Hz, azulene ring), 7.80 (d, 1H, J = 4.0 Hz, azulene ring), 7.54 (t, 1H, J = 10 Hz, azulene ring), 7.34 (d, 1H, J = 3.5 Hz, azulene ring), 7.09 (t, 1H, J = 10 Hz, azulene ring), 7.07 (t, 1H, J = 10 Hz, azulene ring), 3.72 (dt, 2H, J = 6.0 Hz, −CH_2−), 3.18 (t, 2H, J = 7.5 Hz, −CH_2−), 2.04 (tt, 2H, J = 7.0 Hz, −CH_2−).

3-(Azulen-1-yl)-1-propyl Methanesulfonate (Az−$(CH_2)_3$-OSO_2CH_3). A mixture of Az−$(CH_2)_3$OH (0.0243 g, 0.134 mmol) and methanesulfonyl chloride (0.0460 g, 0.402 mmol) was dissolved in dry pyridine (10 mL). The mixture was stirred under nitrogen for 30 min, then washed with 1 N HCl, extracted with dichloromethane, and evaporated, yielding 0.0326 g (0.116 mmol, 87%) of Az−$(CH_2)_3OSO_2CH_3$. ^{1}H NMR (δ in $CDCl_3$): 8.27 (d, 2H, J = 9.5 Hz, azulene ring), 7.79 (d, 1H, J = 4.0 Hz, azulene ring), 7.56 (t, 1H, J = 10 Hz, azulene ring), 7.35 (d, 1H, J = 3.5 Hz, azulene ring), 7.13 (t, 1H, J = 9.5 Hz, azulene ring), 7.10 (t, 1H, J = 9.5 Hz, azulene ring), 4.24 (t, 2H, J = 6.5 Hz, Az−CH_2−), 3.23 (t, 2H, J = 8.0 Hz, −CH_2−OSO_2−), 2.96 (s, 3H, −CH_3), 2.22 (tt, 2H, J = 7.0 Hz, −CH_2−).

1-(Azulen-1-yl)-3-idopropane (Az−$(CH_2)_3$I). Az−$(CH_2)_3$-OSO_2CH_3 (0.0326 g, 0.116 mmol) was added to the saturated sodium iodide/acetone solution (10 mL). This mixture was heated to reflux in an oil bath under nitrogen with stirring for 2 h. The mixture was washed with water, extracted with dichloromethane, and evaporated, yielding 0.0283 g (0.0956 mmol, 82%) of Az−$(CH_2)_3$I. ^{1}H NMR (δ in $CDCl_3$): 8.32 (d, 1H, J = 9.5 Hz, azulene ring), 8.26 (d, 1H, J = 9 Hz, azulene ring), 7.79 (d, 1H, J = 3.5 Hz, azulene ring), 7.55 (t, 1H, J = 10 Hz, azulene ring), 7.34 (d, 1H, J = 4.5 Hz, azulene ring), 7.12 (t, 1H, J = 9.5 Hz, azulene ring), 7.09 (t, 1H, J = 10 Hz, azulene ring), 3.20 (t, 4H, J = 7.0 Hz, Az−CH_2− and −CH_2I), 2.27 (tt, 2H, J = 7.0 Hz, −CH_2−). Mass spectrum: 296 (calcd for M$^+$: 296).

7-((3-(Azulen-1-yl)propyl)amino)-4-trifluoromethylcoumarin (Az−$(CH_2)_3$−C151). A mixture of Az−$(CH_2)_3$I (0.0283 g, 0.0956 mmol), C151 (0.0219 g, 0.0956 mmol), and potassium carbonate (0.0264 g, 0.191 mmol) was dissolved in butylnitrile (10 mL). The mixture was heated to reflux under nitrogen for 1.5 days. The crude product was dissolved in benzene, and the dark solid was removed by filtration. The filtrate was chromatographed on silica gel with dichloromethane. The green fraction was collected and evaporated, to yield 0.0015 g (0.0038 mmol, 4.0%) of Az−$(CH_2)_3$−C151. ^{1}H NMR (δ in

$CDCl_3$): 8.28 (d, 1H, $J = 9.0$ Hz, azulene ring), 8.25 (d, 1H, $J = 10$ Hz, azulene ring), 7.78 (d, 1H, $J = 3.5$ Hz, azulene ring), 7.55 (t, 1H, $J = 10$ Hz, azulene ring), 7.40 (dd, 1H, $J = 9.0$ Hz, 2.0 Hz, coumarin ring), 7.36 (d, 1H, $J = 4.0$ Hz, azulene ring), 7.10 (t, 1H, $J = 9.5$ Hz, azulene ring), 7.08 (t, 1H, $J = 10.5$ Hz, azulene ring), 6.40 (m, 3H, coumarin ring), 5.27 (s, 1H, −NH−), 4.30 (d, 2H, $J = 7.0$ Hz, Az−CH_2−), 3.24 (dt, 2H, −CH_2−), 2.14 (tt, 2H, $J = 7.0$ Hz, −CH_2−). Mass spectrum: 397 (calcd for M^+: 397).

Acknowledgment. We thank Dr. Y. Kimura (Kyoto University) for his kind help with the transient and the steady-state absorption measurements. We also thank Professor H. Furuta (Kyoto University) for his kind help with the organic synthesis. T.O. wishes to thank the Japan Society for the Promotion of Science.

References and Notes

(1) (a) Seilmeier, A.; Kaiser, W. In *Ultrashort laser pulses and applications*, 2nd ed.; Kaiser, W., Ed.; Springer-Verlag: New York, 1993. (b) Elsaesser, T.; Kaiser, W. *Annu. Rev. Phys. Chem.* **1991**, *42*, 83.
(2) Baker, J. R. *J. Phys. Chem.* **1984**, *88*, 11.
(3) Hippler, H.; Lindemann, L.; Troe, J. *J. Chem. Phys.* **1985**, *83*, 3906.
(4) Brouwer, L.; Hippler, H.; Lindemann, L.; Troe, J. *J. Phys. Chem.* **1985**, *89*, 4608.
(5) Hold, U.; Lenzer, T.; Luther, K.; Reihs, K.; Symonds, A. *Ber. Bunsen-Ges. Phys. Chem.* **1997**, *101*, 552.
(6) Wild, W.; Seilmeier, A.; Gottfried, N. H.; Kaiser, W. *Chem. Phys. Lett.* **1985**, *119*, 259.
(7) Sukowski, U.; Seilmeier, A.; Elsaesser, T.; Fischer, S. F. *J. Chem. Phys.* **1990**, *93*, 4094.
(8) Schultz, K. E.; Russell, D. J.; Harris, C. B. *J. Chem. Phys.* **1992**, *97*, 5431.
(9) Schwarzer, D.; Troe, J.; Votsmeier, M.; Zerezke, M. *J. Chem. Phys.* **1996**, *105*, 3121.
(10) Schwarzer, D.; Troe, J.; Votsmeier, M.; Zerezke, M. *Ber. Bunsen-Ges. Phys. Chem.* **1997**, *101*, 595.
(11) Schwarzer, D.; Troe, J.; Zerezke, M. *J. Chem. Phys.* **1997**, *107*, 8380.
(12) Schwarzer, D.; Troe, J.; Zerezke, M. *J. Phys. Chem. A* **1998**, *102*, 4207.
(13) Hidelbach, C.; Fedchenia, I. I.; Schwarzer, D.; Schroeder, J. *J. Chem. Phys.* **1998**, *108*, 10152.
(14) Hidelbach, C.; Schroeder, J.; Schwarzer, D.; Vikhrenko, V. S. *Chem. Phys. Lett.* **1998**, *291*, 333.
(15) Schwarzer, D.; Troe, J.; Schroeder, J. *Ber. Bunsen-Ges. Phys. Chem.* **1991**, *95*, 933.
(16) Wagner, B. D.; Szymanski, M.; Steer, R. P. *J. Chem. Phys.* **1993**, *98*, 301.
(17) Proceedings of the international conference on photoacoustic and photothermal phenomena. *J. Phys.* **1994**, *4*, C7; *Prog, Natural Sci.* **1996**, *6*.
(18) Terazima, M. *J. Chem. Phys.* **1996**, *105*, 6587.
(19) Okazaki, T.; Hirota, N.; Terazima, M. *J. Phys. Chem. A* **1997**, *101*, 650.
(20) Takezaki, M.; Hirota, N.; Terazima, M. *J. Phys. Chem. A* **1997**, *101*, 3443.
(21) Terazima, M.; Takezaki, M.; Yamaguchi, S.; Hirota, N. *J. Chem. Phys.* **1998**, *109*, 603.
(22) Terazima, M. *Chem. Phys. Lett.* **1999**, *305*, 189.
(23) Okazaki, T.; Hirota, N.; Terazima, M. *J. Chem. Phys.* **1999**, *110*, 11399.
(24) Okazaki, T.; Hirota, N.; Nagata, T.; Osuka, A.; Terazima, M. *J. Am. Chem. Soc.* **1999**, *121*, 5079.
(25) Kimura, Y.; Takebayashi, Y.; Hirota, N. *J. Chem. Phys.* **1998**, *108*, 1485.
(26) Yoshimura, Y.; Osugi, J.; Nakahara, M. *J. Am. Chem. Soc.* **1983**, *105*, 5414.
(27) Tanaka, Y.; Yamamoto, T.; Satomi, Y.; Kubota, H.; Makita, T. *Rev. Phys. Chem. Jpn.* **1977**, *47*, 12.
(28) Gustavsson, T.; Cassara, L.; Gulbinas, V.; Gurzadyan, G.; Mialocq, J.-C.; Pommeret, S.; Sorgius, M.; van der Meulen, P. *J. Phys. Chem. A* **1998**, *102*, 4229.
(29) Seilmeier, A.; Scherer, P. O. J.; Kaiser, W. *Chem. Phys. Lett.* **1984**, *105*, 140.
(30) Gottfried, N. H.; Seilmeier, A.; Kaiser, W. *Chem. Phys. Lett.* **1984**, *111*, 326.
(31) Sension, R. J.; Repinec, S. T.; Hochstrasser, R. M. *J. Chem. Phys.* **1990**, *93*, 9185.
(32) Hagan, T.; Pilloud, D.; Suppan, P. *Chem. Phys. Lett.* **1987**, *139*, 499.
(33) Suppan, P. *J. Photochem. Photobiol. A: Chem.* **1990**, *50*, 293.
(34) Scherer, P. O. J.; Seilmeier, A.; Kaiser, W. *J. Chem. Phys.* **1985**, *83*, 3948.
(35) Rosenthal, S. J.; Xie, X.; Du, M.; Fleming, G. R. *J. Chem. Phys.* **1991**, *95*, 4715.
(36) Cho, M.; Rosenthal, S. J.; Scherer, N. F.; Ziegler, L. D.; Fleming, G. R. *J. Chem. Phys.* **1992**, *96*, 5033.
(37) Jimenez, R.; Fleming, G. R.; Kumar, P. V.; Maroncelli, M. *Nature* **1994**, *369*, 471.
(38) Kumar, P. V.; Maroncelli, M. *J. Chem. Phys.* **1995**, *103*, 3038.
(39) Gardecki, J.; Horng, M. L.; Papazyan, A.; Maroncelli, M. *J. Mol. Liq.* **1995**, *65/66*, 49.
(40) Horng, M. L.; Gardecki, J. A.; Papazyan, A.; Maroncelli, M. *J. Phys. Chem.* **1995**, *99*, 17311.
(41) Carslaw, H. S.; Jaeger, J. C. *Conduction of Heat in Solids*, 2nd ed.; Oxford University: Oxford, U.K., 1959.
(42) *Handbook of Chemistry and Physics*, 73rd ed.; CRC Press: Boca Raton, 1992.
(43) Edward, J. T. *J. Chem. Educ.* **1970**, *47*, 261.
(44) Mourits, F. M.; Rummens, F. H. A. *Can. J. Chem.* **1979**, *55*, 3010.
(45) Nagaoka, M.; Okuno, Y.; Yamabe, T. *J. Phys. Chem.* **1994**, *98*, 12506.
(46) Sension, R. J.; Szarka, A. Z.; Hochstrasser, R. M. *J. Chem. Phys.* **1992**, *97*, 5239.
(47) Lenz, K.; Pfeiffer, M.; Lau, A.; Elsaesser, T. *Chem. Phys. Lett.* **1994**, *229*, 340.
(48) Qian, J.; Schultz, S. L.; Jean, J. M. *Chem. Phys. Lett.* **1995**, *233*, 9.
(49) Shreve, A. P.; Mathies, R. A. *J. Phys. Chem.* **1995**, *99*, 7285.
(50) Mizutani, Y.; Kitagawa, T. *Science* **1997**, *278*, 443.
(51) (a) Nakabayashi, T.; Okamoto, H.; Tasumi, M. *J. Phys. Chem. A* **1997**, *101*, 7189. (b) Nakabayashi, T.; Okamoto, H.; Tasumi, M. *J. Phys. Chem. A* **1998**, *102*, 9686.
(52) McDowell, D. R.; Wu, F.; Weisman, R. B. *J. Chem. Phys.* **1998**, *108*, 9404.
(53) Ohmine, I. *J. Chem. Phys.* **1986**, *85*, 3342.
(54) Klçn, P.; Wagner, P. J. *J. Am. Chem. Soc.* **1998**, *120*, 2198.
(55) Hisada, K.; Tsuchida, A.; Ito, S.; Yamamoto, M. *J. Phys. Chem. B* **1998**, *102*, 2640.
(56) Wagner, P. J.; El-Taliawi, G. M. *J. Am. Chem. Soc.* **1992**, *114*, 8325.
(57) Lewis, F. D.; Wagner-Brennan, J. M.; Denari, J. M. *J. Phys. Chem. A* **1998**, *102*, 519.
(58) Hafner, K.; Bernhard, C. *Ann. Chim.* **1959**, *625*, 108.